Enhancing Performance of Nonfullerene Acceptors via Side-Chain Conjugation Strategy

Jiayu Wang, Wei Wang, Xiaohui Wang, Yang Wu, Qianqian Zhang, Cenqi Yan, Wei Ma, Wei You, and Xiaowei Zhan*

A side-chain conjugation strategy in the design of nonfullerene electron acceptors is proposed, with the design and synthesis of a side-chain-conjugated acceptor (ITIC2) based on a 4,8-bis(5-(2-ethylhexyl)thiophen-2-yl)benzo[1,2-*b*:4,5-*b'*]di(cyclopenta-dithiophene) electron-donating core and 1,1-dicyanomethylene-3-indanone electron-withdrawing end groups. ITIC2 with the conjugated side chains exhibits an absorption peak at 714 nm, which redshifts 12 nm relative to ITIC1. The absorption extinction coefficient of ITIC2 is 2.7×10^5 M^{-1} cm^{-1}, higher than that of ITIC1 (1.5×10^5 M^{-1} cm^{-1}). ITIC2 exhibits slightly higher highest occupied molecular orbital (HOMO) (−5.43 eV) and lowest unoccupied molecular orbital (LUMO) (−3.80 eV) energy levels relative to ITIC1 (HOMO: −5.48 eV; LUMO: −3.84 eV), and higher electron mobility (1.3×10^{-3} cm^2 V^{-1} s^{-1}) than that of ITIC1 (9.6×10^{-4} cm^2 V^{-1} s^{-1}). The power conversion efficiency of ITIC2-based organic solar cells is 11.0%, much higher than that of ITIC1-based control devices (8.54%). Our results demonstrate that side-chain conjugation can tune energy levels, enhance absorption, and electron mobility, and finally enhance photovoltaic performance of nonfullerene acceptors.

Organic solar cells (OSCs) have been considered as a promising alternative to silicon-based solar cells since they present some merits such as light weight, low cost, semitransparency, flexibility, and large-area fabrication.[1–6] The active layers in bulk heterojunction (BHJ) OSCs consist of electron donors and electron acceptors.[7,8] Fullerenes and their derivatives possess some advantages, such as large electron affinity, high electron mobility, and isotropic charge transport, and are the dominating acceptor materials during the past two decades.[9] However,

J. Wang, W. Wang, C. Yan, Prof. X. Zhan
Department of Materials Science and Engineering
College of Engineering
Key Laboratory of Polymer Chemistry and Physics of Ministry of Education
Peking University
Beijing 100871, China
E-mail: xwzhan@pku.edu.cn
X. Wang, Y. Wu, Prof. W. Ma
State Key Laboratory for Mechanical Behavior of Materials
Xi'an Jiaotong University
Xi'an 710049, China
Q. Zhang, Prof. W. You
Department of Chemistry
University of North Carolina at Chapel Hill
Chapel Hill, NC 27599-3290, USA

since fullerenes suffer from some shortcomings, such as weak absorption in the visible region, limited energy level tunability, and high cost, the improvement of fullerene-based OSCs mainly relies on donor refinement, which may restrict the further development of the OSCs.[10,11]

Nonfullerene acceptors for BHJ OSCs have been investigated for a decade.[12–14] In the past two years, nonfullerene acceptors have realized significant development with power conversion efficiency (PCE) increasing from 6%[15–23] to 12%.[24–26] Rylene imides/amides[27–35] and fused-ring electron acceptors (FREAs)[19,20,24–26,36–47] are two categories of promising materials. Parent rylene imides/amides usually possess high planarity and strong intermolecular interaction, and form large crystalline domains and large phase separation in BHJ films, leading to reduced exciton diffusion/s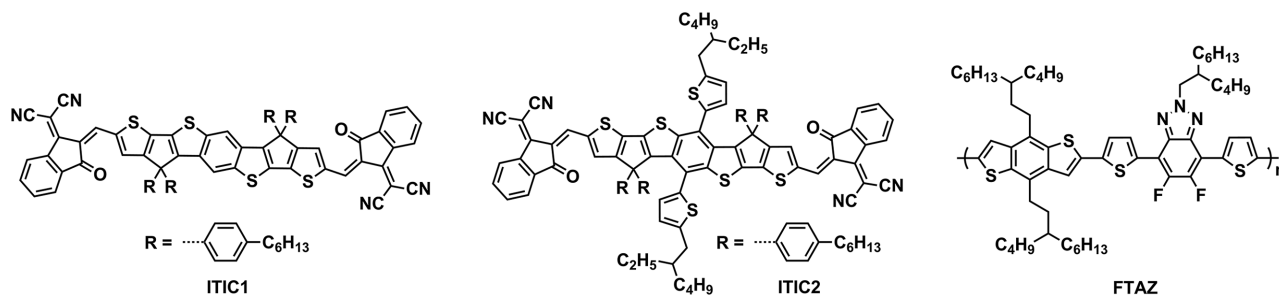eparation efficiencies and low PCEs.[48,49] Thus, the design strategy of high-performance rylene imide/amide-based acceptors is to restrict planarity and crystallinity by forming twisted or 3D structures.[50,51] The OSCs based on 3D rylene imide/amide acceptors exhibit PCEs up to 9%.[32,33,52]

Recently, we proposed the concept of "fused-ring electron acceptor" and reported a series of FREAs based on a fused-ring electron-donating core, such as indacenodithiophene, indacenodithieno[3,2-*b*]thiophene, and indacenobis(dithieno[3,2-*b*;2',3'-*d*]thiophene), flanked with two compact strong electron-withdrawing units such as 1,1-dicyanomethylene-3-indanone (IC) and halogenated IC.[19,20,26,46,53–55] These FREAs present strong absorption in the visible and near-infrared region, and tunable and appropriate energy levels matching with various high-performance donor materials.[56] Owing to the planar molecular backbone, especially the compact acceptor units at the ends, there is a strong intermolecular interaction, endowing FREAs with relatively high electron mobility.[57] The side chains on the fused-ring core are linked to the sp^3 carbon atom of the cyclopentadiene moiety and adopt out-of-plane orientation, which can inhibit excessive aggregation of the molecules.

Polymer donors with conjugated side chains (also called 2D conjugated polymer donors) are widely used in OSCs and usually exhibit superior performance relative to their counterparts without conjugated side chains.[58,59] Inspired by the superior

Scheme 1. Chemical structures of ITIC1, ITIC2, and FTAZ.

performance of these materials, we introduce conjugated side chains onto the molecular backbone of nonfullerene acceptors (2D conjugated acceptors). The benefits of side chain conjugation are as follows: (1) extending the intramolecular conjugation, which would extend and enhance the absorption, resulting in higher photocurrent; (2) facilitating intermolecular interaction and π–π overlap, resulting in higher charge carrier mobility.

In this work, we present the first example of FREA with conjugated side chains, design and synthesize an acceptor with conjugated side chains, ITIC2 (**Scheme 1**), and compare with its counterpart, ITIC1 (Scheme 1). ITIC2 consists of an electron-rich benzo[1,2-*b*:4,5-*b*′]di(cyclopenta[2,1-*b*:3,4-*b*′]dithiophene) core, electron-deficient IC end groups, conjugated 5-(2-ethyl-hexyl)thiophene side chains, and nonconjugated 4-hexylbenzene side chains. ITIC2 exhibits redshifted and stronger absorption, higher energy levels, and higher electron mobility relative to ITIC1. The OSCs based on blends of ITIC2 and a wide-bandgap polymer donor FTAZ[60] (Scheme 1) show a champion PCE of 11.0%, much higher than ITIC1-based devices (8.54%).

The molecular geometries and electronic properties of ITIC1 and ITIC2 were investigated with density functional theory (DFT) calculations at B3LYP/6-31G* level. Both ITIC1 and ITIC2 possess planar backbone (Figure S1, Supporting Information), which would be beneficial to intermolecular π–π interactions, especially local intermolecular π–π stacking between the terminal electron-deficient IC groups, facilitating electron transport.[57] The highest occupied molecular orbital (HOMO) of the two molecules mainly distributes on the electron-donating core, and the lowest unoccupied molecular orbital (LUMO) delocalized on the whole molecular backbone (Figure S1, Supporting Information). Furthermore, the HOMO and HOMO-1 of ITIC2 extend into the thiophene side chains, indicating that the thiophene side chains and the molecular backbone are conjugated. The calculated HOMO and LUMO energy levels of ITIC2 are −5.36 and −3.34 eV, respectively, higher than those

of ITIC1 (HOMO: −5.45 eV; LUMO: −3.39 eV), which could be attributed to the electron-donating property of conjugated thiophene units in side chains.

Scheme S1 (Supporting Information) shows the synthetic routes for ITIC2. Pd(PPh₃)₄ catalyzed Stille coupling reaction between BDT2-2Sn and ethyl 2-bromothiophene-3-carboxylate afforded intermediate BDT2-T. Grignard reaction between BDT2-T and 4-hexylphenyl-1-magnesium bromide followed by intramolecular cyclization via acid-mediated Friedel–Crafts reaction afforded IT2. IT2 was lithiated by *n*-butyllithium and quenched with dimethylformamide to afford aldehyde IT2-CHO. Knoevenagel condensation between IT2-CHO and IC yielded the final product ITIC2. ITIC1 was synthesized from the known starting material IT1[61] using the same procedure as ITIC2, which is different from the reported procedure (ITIC1 was coincidentally reported while we were preparing this paper).[62] All compounds were fully characterized by mass spectrometry, ¹H NMR, ¹³C NMR, and elemental analysis (see the Supporting Information).

ITIC1 and ITIC2 are readily soluble in common organic solvents, such as dichloromethane and chloroform. Thermogravimetric analysis (Figure S2, Supporting Information) indicates that ITIC1 and ITIC2 possess good thermal stability with decomposition temperatures (5% weight loss) of 360 and 339 °C in nitrogen, respectively (**Table 1**).

The normalized optical absorption spectra of ITIC1 and ITIC2 in chloroform solution (10⁻⁶ M⁻¹) and thin film are shown in **Figure 1**a. The two compounds exhibit strong and broad absorption ranging from 550 to 800 nm. ITIC1 shows an absorption maximum at 702 nm with an extinction coefficient of 1.5×10^5 M⁻¹ cm⁻¹ in solution, while ITIC2 with the conjugated side chains shows a redshifted maximum at 714 nm and a higher extinction coefficient of 2.7×10^5 M⁻¹ cm⁻¹. ITIC1 and ITIC2 exhibit redshifted absorption spectra in thin film relative to those in solution, with maxima of 734 and 738 nm, respectively. The optical bandgaps of ITIC1 and ITIC2

Table 1. Basic properties of ITIC1 and ITIC2.

Compound	T_d [°C]	λ_{max}^{abs} [nm]		$E_g^{a)}$ [eV]	$\varepsilon^{b)}$ [M⁻¹ cm⁻¹]	$E_{ox}/E_{red}^{c)}$ [V]	HOMO [eV]	LUMO [eV]	μ_e [10⁻⁴ cm² V⁻¹ s⁻¹]
		Solution	Film						
ITIC1	360	702	734	1.55	1.5×10^5	0.68/−0.96	−5.48	−3.84	9.6
ITIC2	339	714	738	1.53	2.7×10^5	0.63/−1.00	−5.43	−3.80	13

a)Estimated from the absorption edge in film; b)Extinction coefficient at λ_{max} in solution; c)The onset oxidation and reduction potentials versus FeCp₂⁺/⁰.
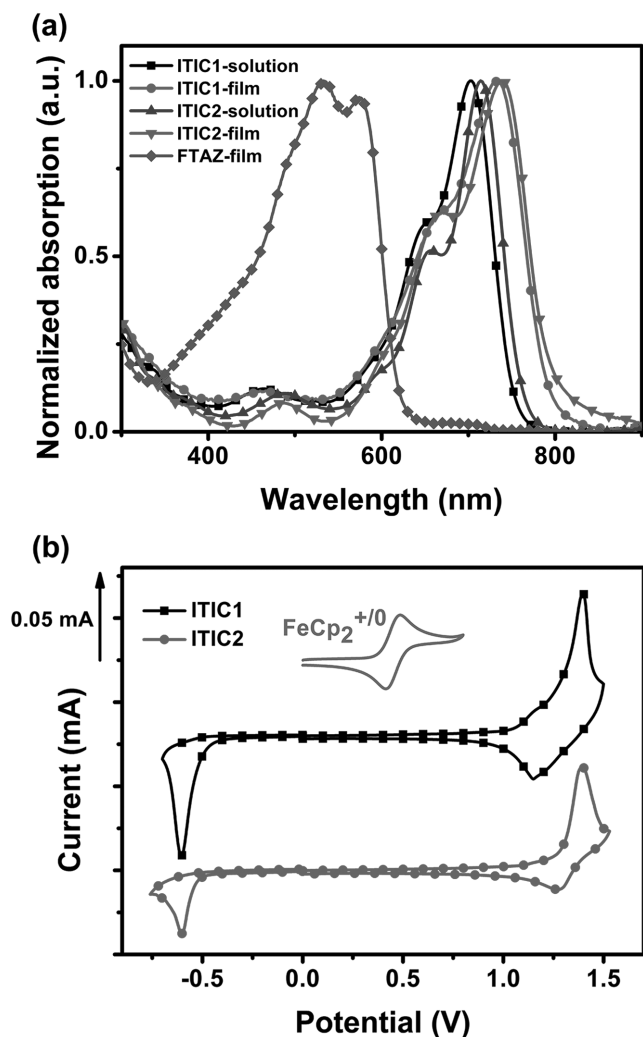
Figure 1. a) UV–vis absorption spectra of ITIC1, ITIC2, and FTAZ. b) Cyclic voltammograms for ITIC1 and ITIC2 in $CH_3CN/0.1$ M $[^nBu_4N]^+[PF_6]^-$ at 100 mV s^{-1}, and the horizontal scale refers to an Ag/AgCl electrode.

estimated from the absorption edge of the thin film are 1.55 and 1.53 eV, respectively (Table 1).

The electrochemical properties of ITIC1 and ITIC2 were investigated by cyclic voltammetry (CV) with films on a glassy carbon working electrode in 0.1 M $[nBu_4N]^+[PF_6]^-$ CH_3CN solution at a potential scan rate of 100 mV s^{-1} (Figure 1b). ITIC1 and ITIC2

exhibit irreversible reduction waves and oxidation waves. The HOMO and LUMO energy levels (Table 1) are estimated from the onset oxidation and reduction potentials, respectively, assuming the absolute energy level of $FeCp_2^{+/0}$ to be 4.8 eV below vacuum (oxidation potential of $FeCp_2^{+/0}$ vs Ag/AgCl was measured to be 0.45 V). ITIC2 shows slightly higher HOMO (−5.43 eV) and LUMO (−3.80 eV) energy levels relative to ITIC1 (HOMO: −5.48 eV; LUMO: −3.84 eV), owing to the electron-donating nature of the conjugated thiophene side chain.

The electron mobilities of ITIC1 and ITIC2 were measured using the space charge limited current (SCLC) method in electron-only devices with a structure of Al/ITIC1 or ITIC2/Al (Figure S3, Supporting Information).[63] The electron mobilities of ITIC1 and ITIC2 are 9.6×10^{-4} and 1.3×10^{-3} cm^2 V^{-1} s^{-1}, respectively (Table 1). The planar molecular backbone of the two molecules facilitates molecular stacking and charge carrier transport, leading to relatively high mobility. The conjugated side chain in ITIC2 could further enhance the intermolecular interaction, resulting in higher mobility.

Our previously reported wide-bandgap (2.00 eV) polymer FTAZ (Scheme 1) exhibits strong absorption from 400 to 620 nm with a high extinction coefficient of 9.8×10^4 M^{-1} cm^{-1}, which is complementary with absorption of the low-bandgap acceptors ITIC1 and ITIC2 (Figure 1a).[60] The energy levels of FTAZ (HOMO = −5.38 eV; LUMO = −3.17 eV)[60] match with those of ITIC1 and ITIC2, and its deep HOMO energy level is beneficial to high open-circuit voltage (V_{OC}). We fabricated BHJ OSCs with a structure of indium tin oxide (ITO)/ZnO/FTAZ: ITIC1 or ITIC2/MoO$_x$/Ag. The optimization details of the devices are illustrated in Table S1 (Supporting Information). **Table 2** summarizes the V_{OC}, short-circuit current density (J_{SC}), fill factor (FF), and PCE of the optimized devices. The current density–voltage ($J–V$) curves of the best devices are shown in **Figure 2**a.

FTAZ:ITIC1-based devices exhibit V_{OC} of 0.921 V, J_{SC} of 16.45 mA cm^{-2}, FF of 0.564, and PCE of 8.54%. Due to the higher LUMO energy level, redshifted and stronger absorption, and higher electron mobility of ITIC2, the devices based on FTAZ:ITIC2 show higher V_{OC} of 0.946 V, higher J_{SC} of 17.51 mA cm^{-2}, higher FF of 0.576, and higher PCE of 9.56%. FTAZ:ITIC1-based devices show slightly decreased performance after thermal annealing (V_{OC} of 0.921 V, J_{SC} of 15.76 mA cm^{-2}, FF of 0.559, and PCE of 8.11%) (Table 2 and Table S1 (Supporting Information)). Thermal annealing significantly enhances the performance of FTAZ:ITIC2-based devices: the J_{SC} and FF are improved to 18.88 mA cm^{-2} and 0.630, respectively, resulting in an increased PCE of 11.0%.

Table 2. Performance and mobilities of the optimized devices based on FTAZ/acceptor.

Device[a]	V_{OC} [V][b]	J_{SC} [mA cm^{-2}][b]	FF[b]	PCE [%][b]	Calculated J_{SC} [mA cm^{-2}]	μ_h [10^{-4} cm^2 V^{-1} s^{-1}]	μ_e [10^{-4} cm^2 V^{-1} s^{-1}]	μ_h/μ_e
FTAZ:ITIC1	0.922 ± 0.003 (0.921)	16.06 ± 0.36 (16.45)	0.562 ± 0.004 (0.564)	8.32 ± 0.19 (8.54)	15.84	27	2.0	13.5
FTAZ:ITIC1[c]	0.920 ± 0.003 (0.921)	15.67 ± 0.18 (15.76)	0.561 ± 0.004 (0.559)	8.09 ± 0.10 (8.11)	15.58	53	2.2	24.1
FTAZ:ITIC2	0.944 ± 0.002 (0.946)	17.01 ± 0.31 (17.51)	0.569 ± 0.005 (0.576)	9.13 ± 0.23 (9.56)	16.79	25	2.1	11.9
FTAZ:ITIC2[c]	0.922 ± 0.003 (0.925)	18.63 ± 0.26 (18.88)	0.620 ± 0.006 (0.630)	10.6 ± 0.2 (11.0)	18.13	14	4.1	3.4

[a]FTAZ:acceptor = 1:1.3 (w/w); [b]Average values with standard deviation were obtained from 20 devices, the values in parentheses are the parameters of the best device; [c]Thermal annealing at 110 °C for 10 min.
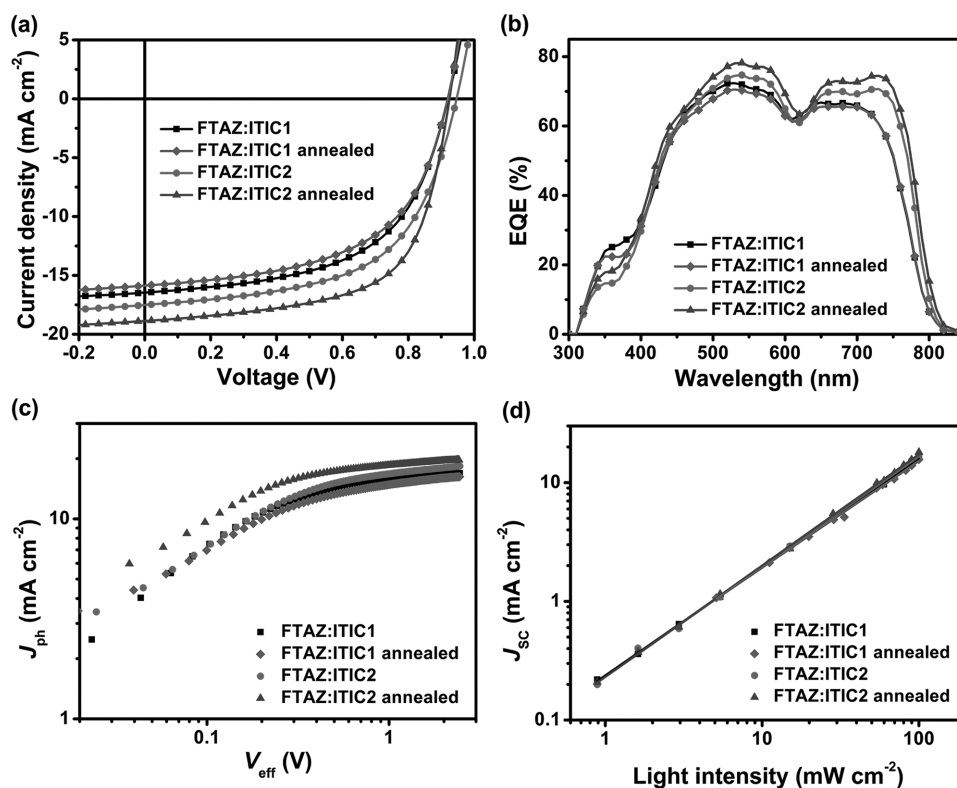
Figure 2. a) J–V curves, b) EQE spectra, c) J_{ph} versus V_{eff} characteristics, and d) J_{SC} versus light intensity of the optimized devices with the structure of ITO/ZnO/FTAZ:acceptor/MoO$_x$/Ag.

The external quantum efficiency (EQE) spectra of the optimized devices exhibit broad photoresponse from 300 to 800 nm (Figure 2b). The photoresponse from 400 to 600 nm is mainly related to the contribution of FTAZ, while that from 600 to 800 nm is mainly attributed to the acceptors. The EQE maxima of FTAZ:ITIC1, annealed FTAZ:ITIC1, FTAZ:ITIC2, and annealed FTAZ:ITIC2 blends are 72.4%, 70.5%, 74.7%, and 78.2%, respectively. FTAZ:ITIC2 shows higher EQE in the 600–800 nm region than FTAZ:ITIC1, which could be ascribed to the stronger absorption of ITIC2, resulting in higher J_{SC}. The J_{SC} of FTAZ:ITIC1, annealed FTAZ:ITIC1, FTAZ:ITIC2, and annealed FTAZ:ITIC2 blends calculated from integration of EQE spectra with the AM 1.5G reference spectrum are 15.84, 15.58, 16.79, and 18.13 mA cm^{-2}, respectively, consistent with J_{SC} values measured from J–V (the error is <5%, Table 2).

We measured the photocurrent density (J_{ph}) versus the effective voltage (V_{eff}) to investigate the charge generation, dissociation, and extraction properties (Figure 2c). Assuming all the photogenerated excitons are dissociated into free charge carriers and collected by electrodes at high V_{eff} (2.2 V), the saturation photocurrent density (J_{sat}) is only limited by the total amount of absorbed incident photons, thus the value of J_{SC}/J_{sat} characterizes the charge extraction under short-circuit condition.[64] The values of J_{SC}/J_{sat} of FTAZ:ITIC1, annealed FTAZ:ITIC1, FTAZ:ITIC2, and annealed FTAZ:ITIC2 blends are >95%, indicating efficient charge extraction.

Charge recombination in the devices was investigated by measuring J_{SC} under different incident light intensities (P_{light})

(Figure 2d). The relationship between J_{SC} and P_{light} can be described by the formula of $J_{SC} \propto P^{S}$.[65] If all free carriers are swept out and collected at the electrodes prior to recombination, S should be equal to 1, while $S < 1$ indicates some extent of bimolecular recombination. The values of S in FTAZ:ITIC1, annealed FTAZ:ITIC1, FTAZ:ITIC2, and annealed FTAZ:ITIC2 blends are 0.92, 0.90, 0.93, and 0.95, respectively, which indicates weak bimolecular recombination and is consistent with the trend of device performance.

The hole and electron mobilities of the blended films were measured by the SCLC method with a device structure of ITO/PEDOT:PSS/FTAZ:acceptor/Au for holes (Figure S4a, Supporting Information) and Al/FTAZ:acceptor/Al for electrons (Figure S4b, Supporting Information). Devices based on FTAZ:ITIC1 (μ_h = 2.7 × 10^{-3} cm^2 V^{-1} s^{-1}, μ_e = 2.0 × 10^{-4} cm^2 V^{-1} s^{-1}) and FTAZ:ITIC2 (μ_h = 2.5 × 10^{-3} cm^2 V^{-1} s^{-1}, μ_e = 2.1 × 10^{-4} cm^2 V^{-1} s^{-1}) exhibit similar hole and electron mobilities. After thermal annealing, the hole mobility of FTAZ:ITIC1 significantly increases to 5.3 × 10^{-3} cm^2 V^{-1} s^{-1}, while the electron mobility slightly increases to 2.2 × 10^{-4} cm^2 V^{-1} s^{-1}. As for the FTAZ:ITIC2 annealed film, the hole mobility decreases down to 1.4 × 10^{-3} cm^2 V^{-1} s^{-1}, while the electron mobility increases up to 4.1 × 10^{-4} cm^2 V^{-1} s^{-1} (Table 2). The slightly lower J_{SC} and slightly lower FF of the annealed FTAZ:ITIC1 blend relative to its as-cast film could be attributed to the unbalanced charge transport, while the higher J_{SC} and FF in the annealed FTAZ:ITIC2 blend relative to its as-cast film could be attributed to the higher electron mobility and more balanced charge transport.[66–70]
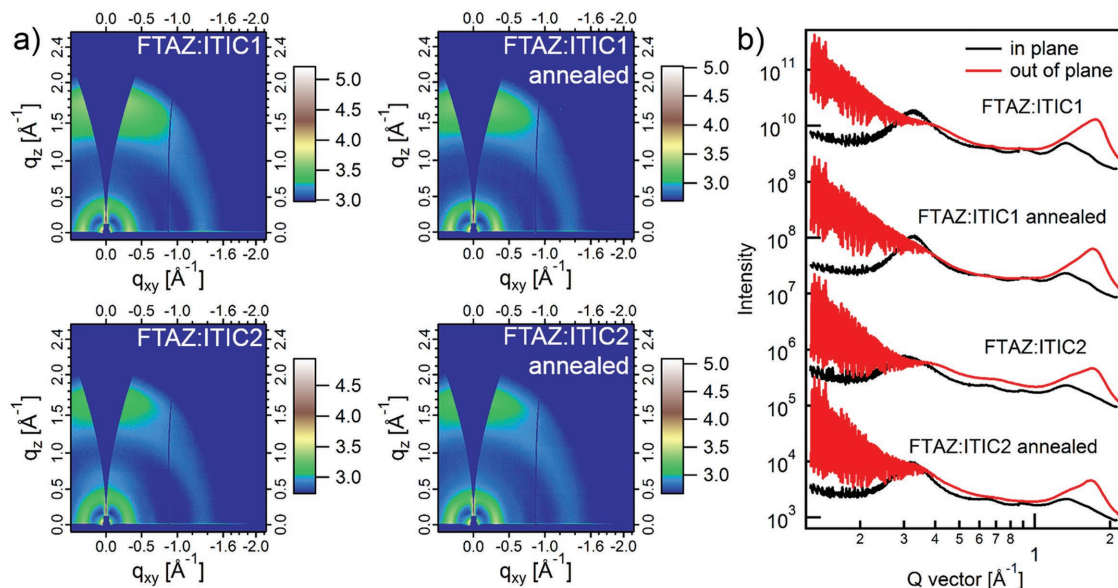
Figure 3. a) 2D GIWAXS patterns of FTAZ:ITIC1, FTAZ:ITIC1 annealed, FTAZ:ITIC2, and FTAZ:ITIC2 annealed films. b) Out-of-plane and in-plane intensity profiles of the corresponding 2D GIWAXS images.

The morphology of the active layer was investigated by transmission electron microscopy (TEM) and atomic force microscopy (AFM) (Figure S5, Supporting Information). FTAZ:ITIC1 and FTAZ:ITIC2 films show obvious contrast in TEM images, suggesting a large crystallinity difference between donor and acceptor, which would lead to a large mobility difference and unbalanced charge transport. After thermal annealing, the contrast of both films decreases, indicating a reduced crystallinity difference between donor and acceptor. AFM was used to characterize the surface morphology of active layer (Figure S5e–h, Supporting Information). The root-mean-square roughness (R_q) values of FTAZ:ITIC1 and FTAZ:ITIC2 films are 0.972 and 0.809 nm, respectively. Thermal annealing slightly increases the R_q of FTAZ:ITIC1 film to 1.22 nm, while slightly decreases that of FTAZ:ITIC2 film to 0.730 nm. The smooth and uniform surface of active layer indicates that there are no large aggregates or pinholes.

Grazing incidence wide-angle X-ray scattering (GIWAXS) was used to investigate the molecular packing of FTAZ:ITIC1 and FTAZ:ITIC2 films.[71] The scattering of FTAZ, ITIC1, and ITIC2 neat films are shown in Figure S6 (Supporting Information). The (100) lamellar packing of ITIC1 and ITIC2 is located at $q = 0.33$ and 0.30 Å^{-1}, corresponding to the lamellar spacing of ≈19 and ≈21 Å, respectively. The π–π stacking peaks of ITIC1 and ITIC2 are shown at 1.78 Å^{-1} (3.5 Å), while the π–π stacking peak of FTAZ is located at $q = 1.68$ Å^{-1}. The GIWAXS results of FTAZ:ITIC1, FTAZ:ITIC1 annealed, FTAZ:ITIC2, and FTAZ:ITIC2 annealed films are displayed in **Figure 3**. For the as-cast films, the coherence lengths (CLs) of ITIC1 and ITIC2 π–π stacking are calculated to be 2.8 and 3.1 nm, respectively, which indicates that the molecular packing of ITIC2 is slightly enhanced compared with its counterpart. The donor material FTAZ shows similar CL of ≈1.7 nm in the as-cast films of FTAZ:ITIC1 and FTAZ:ITIC2. After thermal annealing, the CLs of FTAZ and ITIC1 π–π stacking are calculated to

be 2.3 and 2.3 nm, respectively, suggesting a reduced crystallinity difference between donor and acceptor. The same trend was observed in the FTAZ: ITIC2 annealed films that the CLs of FTAZ and ITIC2 π–π stacking are calculated to be 2.2 and 2.8 nm, respectively.

Resonant soft X-ray scattering (R-SoXS) was performed to further investigate the phase separation of FTAZ:ITIC1, FTAZ:ITIC1 annealed, FTAZ:ITIC2, and FTAZ:ITIC2 annealed blends with enhanced contrast between different components.[72,73] **Figure 4** shows the scattering profiles of the blends at 285.2 eV. FTAZ:ITIC1 as-cast and annealed films show scattering peaks at $q \sim 0.21$ nm^{-1}, corresponding to the domain size of ≈15 nm. The scattering peak of FTAZ:ITIC2 as-cast film locates at $q \sim 0.31$ nm^{-1}, corresponding to the domain
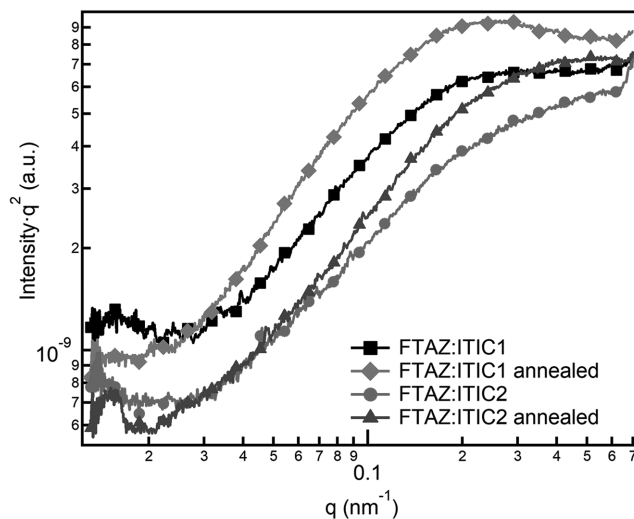

Figure 4. R-SoXS profiles of FTAZ:ITIC1, FTAZ:ITIC1 annealed, FTAZ:ITIC2, and FTAZ:ITIC2 annealed films.

size of ≈10 nm. After thermal annealing, the domain size of FTAZ:ITIC2 slightly reduces to ≈9 nm. The domain sizes of FTAZ:ITIC1 as-cast and annealed films are larger than those of FTAZ:ITIC2 as-cast and annealed films. Smaller domain size facilitates charge separation and higher J_{SC}. Relative domain purity of these blends is also compared by integrating the scattering profiles over q. The relative purity of FTAZ:ITIC1, FTAZ:ITIC1 annealed, FTAZ:ITIC2, and FTAZ:ITIC2 annealed films is calculated to be 0.89, 1, 0.75, and 0.87, respectively. Purer domain of the FTAZ:ITIC1 annealed film with larger domain size would facilitate charge transport but reduce the phase interface, which is beneficial to high mobility but detrimental to charge separation, leading to inferior device performance. For the FTAZ:ITIC2 as-cast and annealed films with smaller domain sizes, high domain purity is beneficial to reducing bimolecular recombination and improving J_{SC} and FF. This is consistent with the results from charge recombination study by measuring J_{SC} versus incident light intensities. Due to the smaller domain size and purer domains, the FTAZ:ITIC2 annealed film shows the highest J_{SC}, FF, and PCE.

In summary, we demonstrate the first example of side-chain-conjugated FREA. Side-chain conjugation facilitates intramolecular conjugation and intermolecular interaction, which is beneficial to absorption and charge transport. Comparing with its counterpart ITIC1, ITIC2 with the conjugated side chains shows redshifted absorption, higher extinction coefficient, slightly higher energy levels, and higher electron mobility. FTAZ:ITIC2 blend shows smaller domain size relative to FTAZ:ITIC1. The OSCs based on FTAZ:ITIC2 blends exhibit a champion PCE of 11.0%, much higher than that of FTAZ:ITIC1 blend (8.54%). The redshifted and stronger absorption of ITIC2 is beneficial to higher J_{SC}, while the higher electron mobility of ITIC2 and more balanced charge transport is beneficial to higher FF. The smaller domain size and high domain purity of FTAZ:ITIC2 blend also facilitate enhancement in J_{SC} and FF. The higher J_{SC} and higher FF synergistically lead to much higher PCE in FTAZ:ITIC2 blends. Our results demonstrate that side-chain conjugation is an effective strategy for design of high-performance nonfullerene acceptors.

Supporting Information

Supporting Information is available from the Wiley Online Library or from the author.

Acknowledgements

Conflict of Interest

The authors declare no conflict of interest.

Keywords

[1] Y.-J. Cheng, S.-H. Yang, C.-S. Hsu, *Chem. Rev.* **2009**, *109*, 5868.
[2] Y. Lin, Y. Li, X. Zhan, *Chem. Soc. Rev.* **2012**, *41*, 4245.
[3] F. C. Krebs, N. Espinosa, M. Hösel, R. R. Søndergaard, M. Jørgensen, *Adv. Mater.* **2014**, *26*, 29.
[4] L. Lu, T. Zheng, Q. Wu, A. M. Schneider, D. Zhao, L. Yu, *Chem. Rev.* **2015**, *115*, 12666.
[5] L. Dou, Y. Liu, Z. Hong, G. Li, Y. Yang, *Chem. Rev.* **2015**, *115*, 12633.
[6] J. Wang, K. Liu, L. Ma, X. Zhan, *Chem. Rev.* **2016**, *116*, 14675.
[7] J. J. M. Halls, C. A. Walsh, N. C. Greenham, E. A. Marseglia, R. H. Friend, S. C. Moratti, A. B. Holmes, *Nature* **1995**, *376*, 498.
[8] G. Yu, J. Gao, J. C. Hummelen, F. Wudl, A. J. Heeger, *Science* **1995**, *270*, 1789.
[9] J. E. Anthony, A. Facchetti, M. Heeney, S. R. Marder, X. Zhan, *Adv. Mater.* **2010**, *22*, 3876.
[10] Y. Lin, X. Zhan, *Mater. Horiz.* **2014**, *1*, 470.
[11] A. Anctil, C. W. Babbitt, R. P. Raffaelle, B. J. Landi, *Environ. Sci. Technol.* **2011**, *45*, 2353.
[12] T. Kietzke, H.-H. Hörhold, D. Neher, *Chem. Mater.* **2005**, *17*, 6532.
[13] R. Y. C. Shin, T. Kietzke, S. Sudhakar, A. Dodabalapur, Z.-K. Chen, A. Sellinger, *Chem. Mater.* **2007**, *19*, 1892.
[14] T. Kietzke, R. Y. C. Shin, D. A. M. Egbe, Z.-K. Chen, A. Sellinger, *Macromolecules* **2007**, *40*, 4424.
[15] Y. Zhong, M. T. Trinh, R. Chen, W. Wang, P. P. Khlyabich, B. Kumar, Q. Xu, C.-Y. Nam, M. Y. Sfeir, C. Black, M. L. Steigerwald, Y.-L. Loo, S. Xiao, F. Ng, X. Y. Zhu, C. Nuckolls, *J. Am. Chem. Soc.* **2014**, *136*, 15215.
[16] Y.-J. Hwang, T. Earmme, B. A. E. Courtright, F. N. Eberle, S. A. Jenekhe, *J. Am. Chem. Soc.* **2015**, *137*, 4424.
[17] J. W. Jung, J. W. Jo, C.-C. Chueh, F. Liu, W. H. Jo, T. P. Russell, A. K. Y. Jen, *Adv. Mater.* **2015**, *27*, 3310.
[18] H. Li, Y.-J. Hwang, B. A. E. Courtright, F. N. Eberle, S. Subramaniyan, S. A. Jenekhe, *Adv. Mater.* **2015**, *27*, 3266.
[19] Y. Lin, J. Wang, Z.-G. Zhang, H. Bai, Y. Li, D. Zhu, X. Zhan, *Adv. Mater.* **2015**, *27*, 1170.
[20] Y. Lin, Z.-G. Zhang, H. Bai, J. Wang, Y. Yao, Y. Li, D. Zhu, X. Zhan, *Energy Environ. Sci.* **2015**, *8*, 610.
[21] C.-H. Wu, C.-C. Chueh, Y.-Y. Xi, H.-L. Zhong, G.-P. Gao, Z.-H. Wang, L. D. Pozzo, T.-C. Wen, A. K. Y. Jen, *Adv. Funct. Mater.* **2015**, *25*, 5326.
[22] J. Zhao, Y. Li, H. Lin, Y. Liu, K. Jiang, C. Mu, T. Ma, J. Y. Lin Lai, H. Hu, D. Yu, H. Yan, *Energy Environ. Sci.* **2015**, *8*, 520.
[23] D. Xia, Y. Wu, Q. Wang, A. Zhang, C. Li, Y. Lin, F. J. M. Colberts, J. J. van Franeker, R. A. J. Janssen, X. Zhan, W. Hu, Z. Tang, W. Ma, W. Li, *Macromolecules* **2016**, *49*, 6445.
[24] S. Li, L. Ye, W. Zhao, S. Zhang, S. Mukherjee, H. Ade, J. Hou, *Adv. Mater.* **2016**, *28*, 9423.
[25] W. Zhao, S. Li, S. Zhang, X. Liu, J. Hou, *Adv. Mater.* **2017**, *29*, 1604059.

[26] F. Zhao, S. Dai, Y. Wu, Q. Zhang, J. Wang, L. Jiang, Q. Ling, Z. Wei, W. Ma, W. You, C. Wang, X. Zhan, *Adv. Mater.* **2017**, *29*, 1700144.

[27] X. Zhan, Z. a. Tan, B. Domercq, Z. An, X. Zhang, S. Barlow, Y. Li, D. Zhu, B. Kippelen, S. R. Marder, *J. Am. Chem. Soc.* **2007**, *129*, 7246.

[28] P. Cheng, L. Ye, X. Zhao, J. Hou, Y. Li, X. Zhan, *Energy Environ. Sci.* **2014**, *7*, 1351.

[29] Y. Zhong, M. T. Trinh, R. Chen, G. E. Purdum, P. P. Khlyabich, M. Sezen, S. Oh, H. Zhu, B. Fowler, B. Zhang, W. Wang, C.-Y. Nam, M. Y. Sfeir, C. T. Black, M. L. Steigerwald, Y.-L. Loo, F. Ng, X. Y. Zhu, C. Nuckolls, *Nat. Commun.* **2015**, *6*, 8242.

[30] D. Meng, D. Sun, C. Zhong, T. Liu, B. Fan, L. Huo, Y. Li, W. Jiang, H. Choi, T. Kim, J. Y. Kim, Y. Sun, Z.-h. Wang, A. J. Heeger, *J. Am. Chem. Soc.* **2015**, *138*, 375.

[31] L. Gao, Z.-G. Zhang, L. Xue, J. Min, J. Zhang, Z. Wei, Y. Li, *Adv. Mater.* **2015**, *28*, 1884.

[32] D. Meng, H. Fu, C. Xiao, X. Meng, T. Winands, W. Ma, W. Wei, B. Fan, L. Huo, N. L. Doltsinis, Y. Li, Y. Sun, Z. Wang, *J. Am. Chem. Soc.* **2016**, *138*, 10184.

[33] Y. Duan, X. Xu, H. Yan, W. Wu, Z. Li, Q. Peng, *Adv. Mater.* **2016**, *29*, 1605115.

[34] Q. Wu, D. Zhao, A. M. Schneider, W. Chen, L. Yu, *J. Am. Chem. Soc.* **2016**, *138*, 7248.

[35] Y.-J. Hwang, H. Li, B. A. E. Courtright, S. Subramaniyan, S. A. Jenekhe, *Adv. Mater.* **2016**, *28*, 124.

[36] W. Wang, C. Yan, T.-K. Lau, J. Wang, K. Liu, Y. Fan, X. Lu, X. Zhan, *Adv. Mater.* **2017**, https://doi.org/10.1002/adma.201701308.

[37] Z. Li, K. Jiang, G. Yang, J. Y. L. Lai, T. Ma, J. Zhao, W. Ma, H. Yan, *Nat. Commun.* **2016**, *7*, 13094.

[38] F. Liu, Z. Zhou, C. Zhang, T. Vergote, H. Fan, F. Liu, X. Zhu, *J. Am. Chem. Soc.* **2016**, *138*, 15523.

[39] N. Qiu, H. Zhang, X. Wan, C. Li, X. Ke, H. Feng, B. Kan, H. Zhang, Q. Zhang, Y. Lu, Y. Chen, *Adv. Mater.* **2017**, *29*, 1604964.

[40] P. Cheng, M. Zhang, T.-K. Lau, Y. Wu, B. Jia, J. Wang, C. Yan, M. Qin, X. Lu, X. Zhan, *Adv. Mater.* **2017**, *29*, 1605216.

[41] H. Yao, Y. Cui, R. Yu, B. Gao, H. Zhang, J. Hou, *Angew. Chem., Int. Ed.* **2017**, *56*, 3045.

[42] D. Baran, R. S. Ashraf, D. A. Hanifi, M. Abdelsamie, N. Gasparini, J. A. Rohr, S. Holliday, A. Wadsworth, S. Lockett, M. Neophytou, C. J. M. Emmott, J. Nelson, C. J. Brabec, A. Amassian, A. Salleo, T. Kirchartz, J. R. Durrant, I. McCulloch, *Nat. Mater.* **2016**, *16*, 363.

[43] H. Bin, L. Gao, Z.-G. Zhang, Y. Yang, Y. Zhang, C. Zhang, S. Chen, L. Xue, C. Yang, M. Xiao, Y. Li, *Nat. Commun.* **2016**, *7*, 13651.

[44] Y. Yang, Z.-G. Zhang, H. Bin, S. Chen, L. Gao, L. Xue, C. Yang, Y. Li, *J. Am. Chem. Soc.* **2016**, *138*, 15011.

[45] W. Zhao, D. Qian, S. Zhang, S. Li, O. Inganäs, F. Gao, J. Hou, *Adv. Mater.* **2016**, *28*, 4734.

[46] S. Dai, F. Zhao, Q. Zhang, T.-K. Lau, T. Li, K. Liu, Q. Ling, C. Wang, X. Lu, W. You, X. Zhan, *J. Am. Chem. Soc.* **2017**, *139*, 1336.

[47] Y. Lin, F. Zhao, Y. Wu, K. Chen, Y. Xia, G. Li, S. K. K. Prasad, J. Zhu, L. Huo, H. Bin, Z.-G. Zhang, X. Guo, M. Zhang, Y. Sun, F. Gao, Z. Wei, W. Ma, C. Wang, J. Hodgkiss, Z. Bo, O. Inganäs, Y. Li, X. Zhan, *Adv. Mater.* **2017**, *29*, 1604155.

[48] X. Zhan, A. Facchetti, S. Barlow, T. J. Marks, M. A. Ratner, M. R. Wasielewski, S. R. Marder, *Adv. Mater.* **2011**, *23*, 268.

[49] X. Guo, A. Facchetti, T. J. Marks, *Chem. Rev.* **2014**, *114*, 8943.

[50] Y. Lin, Y. Wang, J. Wang, J. Hou, Y. Li, D. Zhu, X. Zhan, *Adv. Mater.* **2014**, *26*, 5137.

[51] Y. Lin, X. Zhan, *Acc. Chem. Res.* **2016**, *49*, 175.

[52] J. Liu, S. Chen, D. Qian, B. Gautam, G. Yang, J. Zhao, J. Bergqvist, F. Zhang, W. Ma, H. Ade, O. Inganäs, K. Gundogdu, F. Gao, H. Yan, *Nat. Energy* **2016**, *1*, 16089.

[53] Y. Lin, Q. He, F. Zhao, L. Huo, J. Mai, X. Lu, C.-J. Su, T. Li, J. Wang, J. Zhu, Y. Sun, C. Wang, X. Zhan, *J. Am. Chem. Soc.* **2016**, *138*, 2973.

[54] Y. Lin, F. Zhao, Q. He, L. Huo, Y. Wu, T. C. Parker, W. Ma, Y. Sun, C. Wang, D. Zhu, A. J. Heeger, S. R. Marder, X. Zhan, *J. Am. Chem. Soc.* **2016**, *138*, 4955.

[55] F. Yang, C. Li, W. Lai, A. Zhang, H. Huang, W. Li, *Mater. Chem. Front.* **2017**, https://doi.org/10.1039/C7QM00025A.

[56] Y. Lin, X. Zhan, *Adv. Energy Mater.* **2015**, *5*, 1501063.

[57] G. Han, Y. Guo, X. Song, Y. Wang, Y. Yi, *J. Mater. Chem. C* **2017**, *5*, 4852.

[58] L. Ye, S. Zhang, L. Huo, M. Zhang, J. Hou, *Acc. Chem. Res.* **2014**, *47*, 1595.

[59] Y. Li, Y. Zou, *Adv. Mater.* **2008**, *20*, 2952.

[60] S. C. Price, A. C. Stuart, L. Yang, H. Zhou, W. You, *J. Am. Chem. Soc.* **2011**, *133*, 4625.

[61] Y.-L. Chen, C.-Y. Chang, Y.-J. Cheng, C.-S. Hsu, *Chem. Mater.* **2012**, *24*, 3964.

[62] B. Kan, H. Feng, X. Wan, F. Liu, X. Ke, Y. Wang, Y. Wang, H. Zhang, C. Li, J. Hou, Y. Chen, *J. Am. Chem. Soc.* **2017**, *139*, 4929.

[63] G. G. Malliaras, J. R. Salem, P. J. Brock, C. Scott, *Phys. Rev. B* **1998**, *58*, 13411.

[64] V. D. Mihailetchi, L. J. A. Koster, J. C. Hummelen, P. W. M. Blom, *Phys. Rev. Lett.* **2004**, *93*, 216601.

[65] I. Riedel, J. Parisi, V. Dyakonov, L. Lutsen, D. Vanderzande, J. C. Hummelen, *Adv. Funct. Mater.* **2004**, *14*, 38.

[66] W. Li, S. Albrecht, L. Yang, S. Roland, J. R. Tumbleston, T. McAfee, L. Yan, M. A. Kelly, H. Ade, D. Neher, W. You, *J. Am. Chem. Soc.* **2014**, *136*, 15566.

[67] C. M. Proctor, J. A. Love, T.-Q. Nguyen, *Adv. Mater.* **2014**, *26*, 5957.

[68] J. A. Bartelt, D. Lam, T. M. Burke, S. M. Sweetnam, M. D. McGehee, *Adv. Energy Mater.* **2015**, *5*, 1500577.

[69] D. Bartesaghi, I. d. C. Pérez, J. Kniepert, S. Roland, M. Turbiez, D. Neher, L. J. A. Koster, *Nat. Commun.* **2015**, *6*, 7083.

[70] U. Wurfel, D. Neher, A. Spies, S. Albrecht, *Nat. Commun.* **2015**, *6*, 6951.

[71] H. Alexander, B. Wim, G. James, S. Eric, G. Eliot, K. Rick, M. Alastair, C. Matthew, R. Bruce, P. Howard, *J. Phys.: Conf. Ser.* **2010**, *247*, 012007.

[72] E. Gann, A. T. Young, B. A. Collins, H. Yan, J. Nasiatka, H. A. Padmore, H. Ade, A. Hexemer, C. Wang, *Rev. Sci. Instrum.* **2012**, *83*, 045110.

[73] Y. Wu, Z. Wang, X. Meng, W. Ma, *Prog. Chem.* **2017**, *29*, 93.